Supplement of Biogeosciences, 21, 4699–4715, 2024
https://doi.org/10.5194/bg-21-4699-2024-supplement

Biogeosciences Open Access EGU

Supplement of

Technical note: Comparison of radiometric techniques for estimating recent organic carbon sequestration rates in inland wetland soils

Purbasha Mistry et al.

Correspondence to: Irena F. Creed (irena.creed@utoronto.ca)

Table of Contents

Table S1: Summary of physical characteristics of undisturbed wetlands.

Wetland ID	A-WE-I-W1, A-WE-I-W2, A-CA-I-W3	S-RO-I-W1, S-RO-I-W2, S-LO-I-W3, S-LO-I-W4, S-RO-I-W5, S-RO-I-W6, S-RU-I-W7, S-FO-I-W8, S-FO-I-W9, S-FO-I-W10, S-FO-I-W11, S-FO-I-W12, S-EM-I-W14, S-FO-I-W15, S-FO-I-W16	M-OA-I-W1, M-OA-I-W2, M-OA-I-W3, M-OA-I-W4, M-OA-I-W5	O-BR-I-W1, O-BR-I-W2, O-BR-I-W3, O-AL-I-W4, O-AL-I-W5, O-AL-I-W6
Province	Alberta	Saskatchewan	Manitoba	Ontario
Number of wetlands	3	16	5	6
Latitude and longitude	53.1° to 53.2° N, 113.1° to 113.2° W	51.4° to 51.5° N, 103.7° to 106.7° W	50.1° to 50.2° N, 100.2° to 100.3° W	43.3° to 45.6° N, 74.8° to 80.3° W
Sampling year	2016	2019	2019	2018, 2019
Mean temperature of the growing season (^{0}C)	11	12.1, 11.7	12.4	14.3, 13.8
Mean total annual precipitation of the water year (mm)	439	360, 458	464	892, 997
Hardiness zone	3b	3a - 3b	3a	5a - 5b
Proportion of hardiness	1	1	0.7	0.7 - 1
Soil great group	Black Chernozem	Dark Brown Chernozem, Black Chernozem	Black Chernozem	Grey Brown Luvisol, Humic Gleysol
Soil texture	Fine	Medium	Fine	Coarse, fine
Local surface form	Hummocky and undulating	Hummocky, undulating, and ridged	Hummocky	Hummocky, level
Regional slope (%)	0-9	0-9	4-9	0-15
Drainage class	Well-drained	Well-drained	Well-drained	Well- to Poorly-drained

Table S2: Organic carbon (OC) sequestration rates based on ^{137}Cs and ^{210}Pb dating and their associated classification of 44 sediment cores (where both ^{137}Cs and ^{210}Pb profiles were available).

Wetland sediment core ID	Classification of ^{137}Cs	Classification of ^{210}Pb	OC sequestration rate since 1954, ^{137}Cs (Mg ha^{-1} yr^{-1})	OC sequestration rate since 1963, ^{137}Cs (Mg ha^{-1} yr^{-1})	OC sequestration rate since 1954, ^{210}Pb (Mg ha^{-1} yr^{-1})	OC sequestration rate since 1963, ^{210}Pb (Mg ha^{-1} yr^{-1})
A-WE-I-W2-T3-CW-R3	High-quality	High-quality	1.04	0.62	0.80	0.78
S-RO-I-W1-T3-CW-R3	Low-quality	High-quality	0.32	0.27	0.31	0.33
S-RO-I-W2-T2-CW-R2	High-quality	High-quality	1.62	1.38	0.47	0.49
S-LO-I-W3-T1-CW-R1	High-quality	High-quality	0.64	0.37	0.37	0.40
S-LO-I-W3-T2-CW-R2	High-quality	High-quality	0.56	0.37	0.45	0.50
S-LO-I-W3-T3-CW-R3	High-quality	High-quality	0.47	0.34	0.40	0.43
S-LO-I-W4-T2-CW-R2	High-quality	High-quality	0.93	0.84	0.35	0.36
S-RO-I-W5-T1-CW-R1	High-quality	High-quality	0.84	0.68	0.80	0.83
S-RO-I-W5-T3-CW-R3	High-quality	High-quality	1.00	0.75	0.68	0.70
S-RO-I-W6-T1-CW-R1	Low-quality	Low-quality	0.11	0.05	0.69	0.73
S-RU-I-W7-T1-CW-R1	High-quality	High-quality	0.86	0.55	0.53	0.56
S-RU-I-W7-T2-CW-R2	High-quality	High-quality	0.57	0.30	0.41	0.43
S-RU-I-W7-T3-CW-R3	High-quality	High-quality	0.69	0.60	0.54	0.56
S-FO-I-W8-T2-CW-R2	High-quality	High-quality	1.01	0.83	0.81	0.81
S-FO-I-W8-T3-CW-R3	High-quality	High-quality	0.88	0.83	0.77	0.77
S-FO-I-W9-T2-CW-R2	High-quality	High-quality	0.58	0.34	0.34	0.34
S-FO-I-W9-T3-CW-R3	High-quality	Low-quality	0.44	0.37	0.60	0.63
S-FO-I-W11-T1-CW-R1	High-quality	High-quality	1.70	1.57	1.41	1.36
S-FO-I-W11-T2-CW-R2	High-quality	High-quality	1.31	1.14	0.69	0.71
S-FO-I-W11-T3-CW-R3	High-quality	High-quality	1.04	1.03	0.95	0.95
S-FO-I-W12-T1-CW-R1	High-quality	High-quality	1.25	0.65	1.04	1.04
S-FO-I-W12-T3-CW-R3	High-quality	High-quality	1.16	0.76	0.71	0.71
S-FO-I-W16-T2-CW-R2	High-quality	High-quality	0.67	0.50	0.59	0.60
S-FO-I-W16-T3-CW-R3	High-quality	High-quality	1.18	0.38	0.46	0.46
M-OA-I-W1-T1-CW-R1	High-quality	High-quality	1.60	0.39	0.51	0.53
M-OA-I-W1-T2-CW-R2	High-quality	High-quality	1.11	0.91	0.97	1.01
M-OA-I-W1-T3-CW-R3	High-quality	High-quality	0.99	0.50	0.60	0.63
M-OA-I-W2-T1-CW-R1	High-quality	High-quality	0.98	0.12	1.08	1.15
M-OA-I-W3-T2-CW-R2	High-quality	Low-quality	1.16	0.55	0.50	0.52
M-OA-I-W4-T1-CW-R1	High-quality	High-quality	0.44	0.21	0.34	0.36
M-OA-I-W4-T2-CW-R2	High-quality	High-quality	0.65	0.45	0.43	0.46
M-OA-I-W4-T3-CW-R3	High-quality	Low-quality	0.78	0.06	0.81	0.86
M-OA-I-W5-T1-CW-R1	High-quality	Low-quality	1.03	0.26	0.38	0.39
M-OA-I-W5-T3-CW-R3	High-quality	Low-quality	1.66	1.55	1.80	1.93
O-BR-I-W1-T2-CW-R2	High-quality	High-quality	1.22	0.48	0.74	0.74
O-BR-I-W1-T3-CW-R3	High-quality	High-quality	1.05	0.21	1.03	1.04
O-BR-I-W2-T2-CW-R2	Low-quality	High-quality	0.53	0.21	0.42	0.40
O-BR-I-W2-T3-CW-R3	Low-quality	High-quality	0.26	0.19	0.33	0.36
O-BR-I-W2-T4-CW-R4	Low-quality	High-quality	0.62	0.37	0.55	0.54
O-AL-I-W4-T1-CW-R1	Low-quality	High-quality	0.60	0.10	0.80	0.87
O-AL-I-W4-T2-CW-R2	Low-quality	High-quality	1.14	0.05	0.79	0.74
O-AL-I-W4-T3-CW-R3	High-quality	Low-quality	2.31	1.58	0.73	0.75
O-AL-I-W5-T3-CW-R3	High-quality	High-quality	2.60	0.76	0.76	0.76
O-AL-I-W6-T1-CW-R1	Low-quality	High-quality	1.15	0.12	0.23	0.23

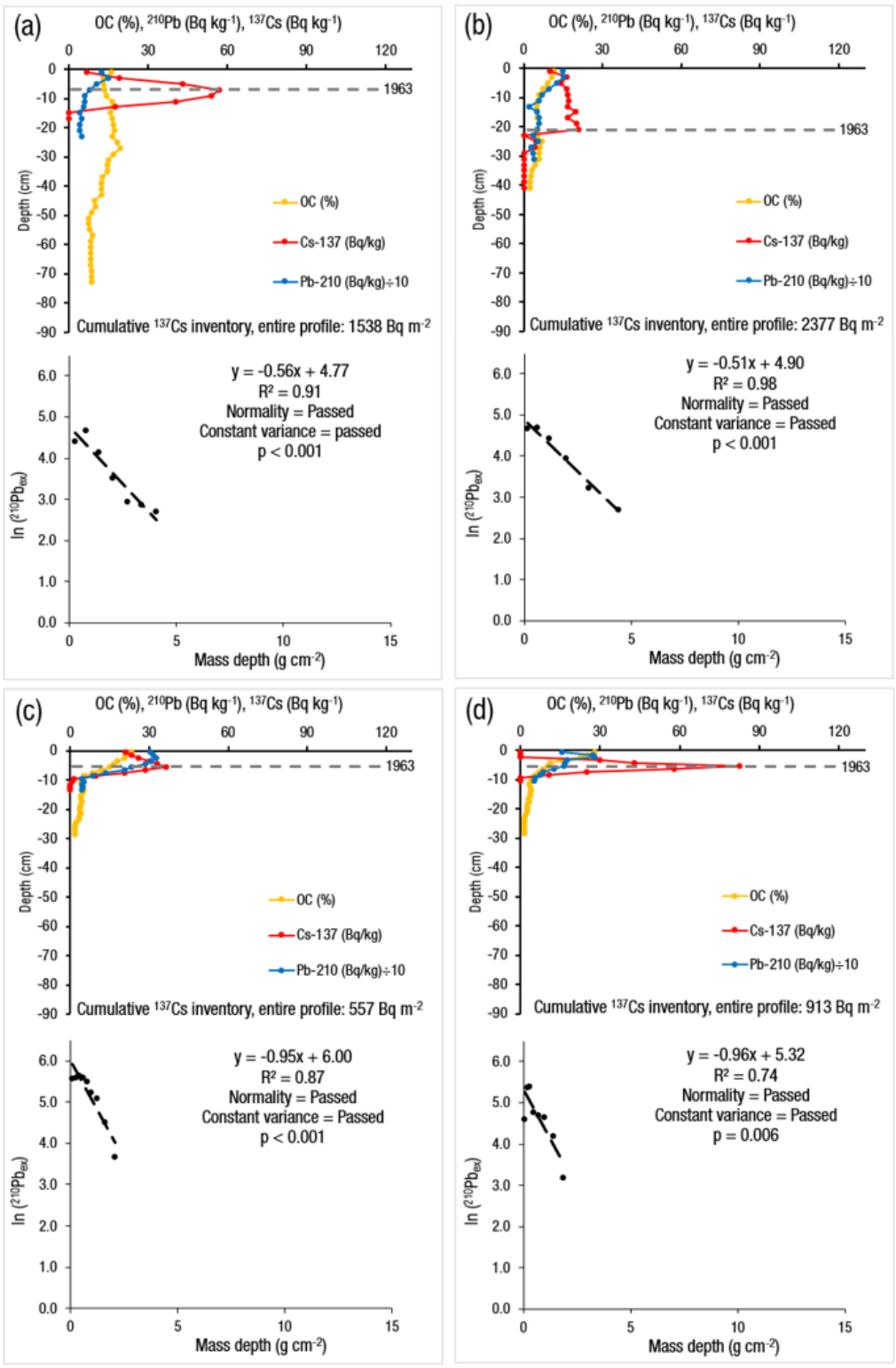

Figure S1: Depth distributions of high-quality ^{137}Cs (Bq kg^{-1}) and high-quality ^{210}Pb (Bq kg^{-1}) profiles (along with the organic carbon [OC] concentrations [%], cumulative ^{137}Cs inventory [Bq m^{-2}], and linear plot of log-transformed ^{210}Pb$_{ex}$ against mass depth [g cm^{-2}]) based on their classification. The four depth distribution plots are from sediment cores (a) A-WE-I-W2-T3-CW-R3, (b) S-RO-I-W2-T2-CW-R2, (c) S-LO-I-W3-T2-CW-R2, and (d) S-LO-I-W3-T3-CW-R3.

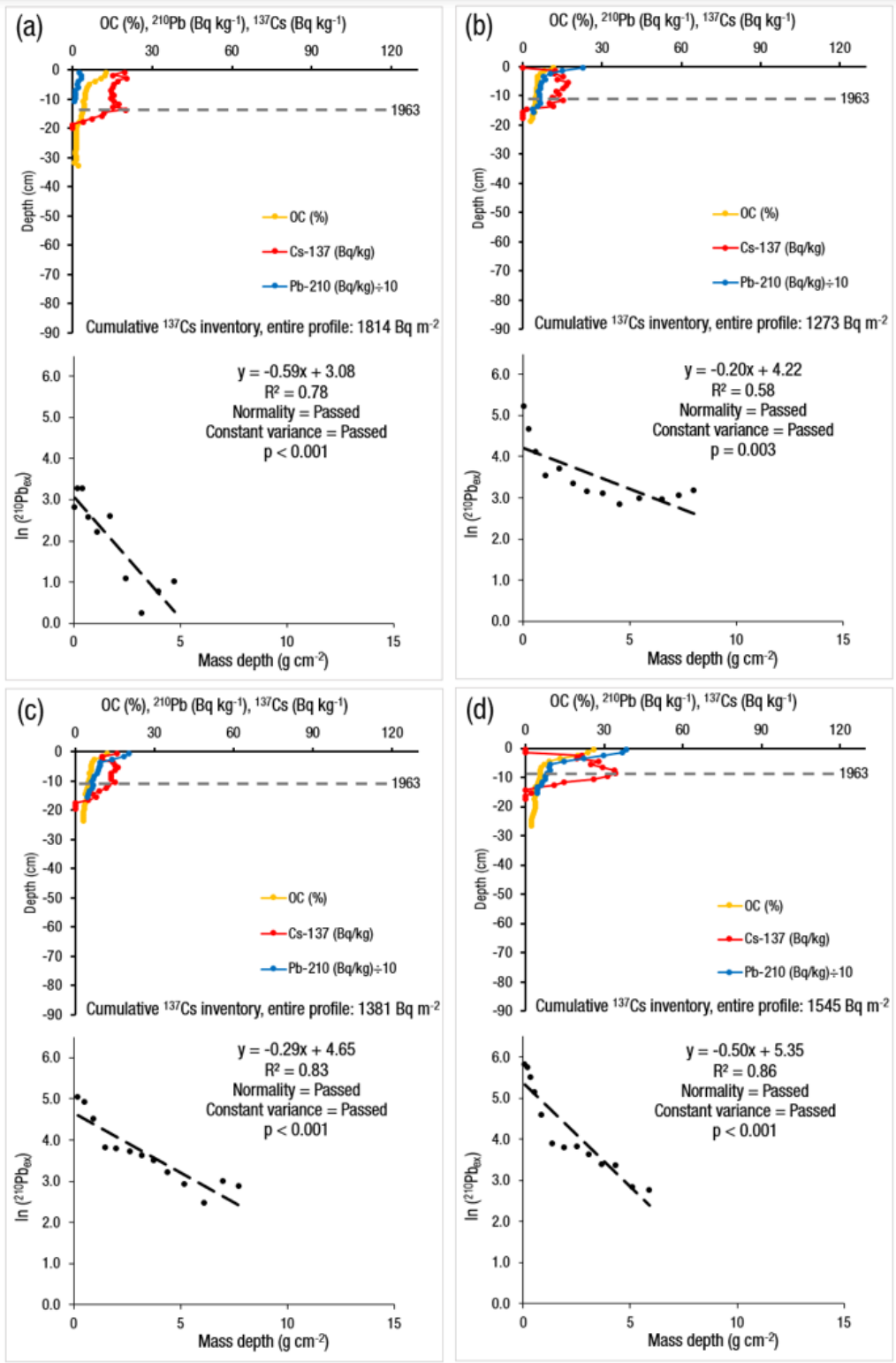

Figure S2: Depth distributions of high-quality ^{137}Cs (Bq kg^{-1}) and high-quality ^{210}Pb (Bq kg^{-1}) profiles (along with the organic carbon [OC] concentrations [%], cumulative ^{137}Cs inventory [Bq m^{-2}], and linear plot of log-transformed ^{210}Pb$_{ex}$ against mass depth [g cm^{-2}]) based on their classification. The four depth distribution plots are from sediment cores (a) S-LO-I-W4-T2-CW-R2, (b) S-RO-I-W5-T1-CW-R1, (c) S-RO-I-W5-T3-CW-R3, and (d) S-RU-I-W7-T1-CW-R1.

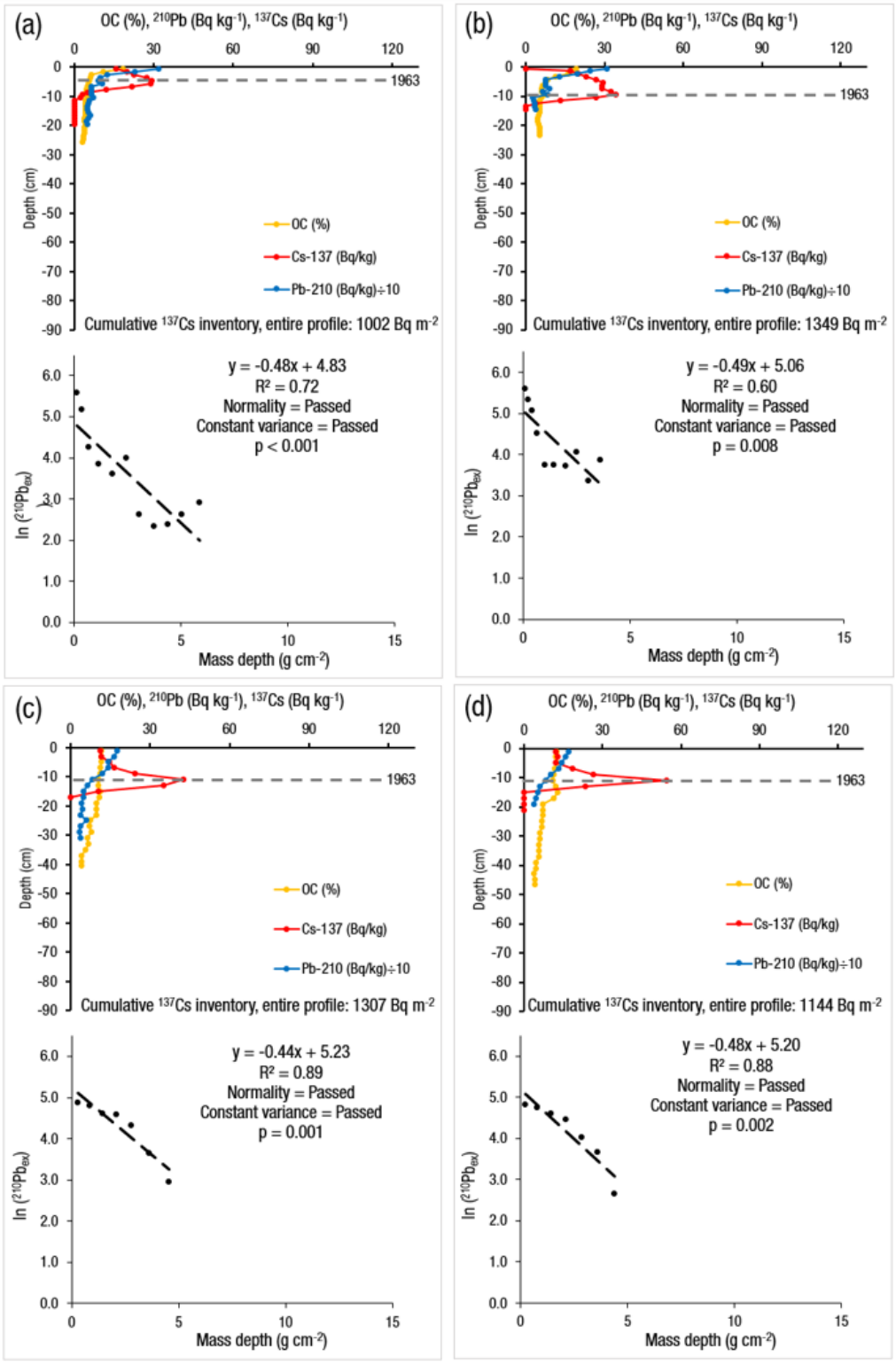

Figure S3: Depth distributions of high-quality ^{137}Cs (Bq kg^{-1}) and high-quality ^{210}Pb (Bq kg^{-1}) profiles (along with the organic carbon [OC] concentrations [%], cumulative ^{137}Cs inventory [Bq m^{-2}], and linear plot of log-transformed ^{210}Pb$_{ex}$ against mass depth [g cm^{-2}]) based on their classification. The four depth distribution plots are from sediment cores (a) S-RU-I-W7-T2-CW-R2, (b) S-RU-I-W7-T3-CW-R3, (c) S-FO-I-W8-T2-CW-R2, and (d) S-FO-I-W8-T3-CW-R3.

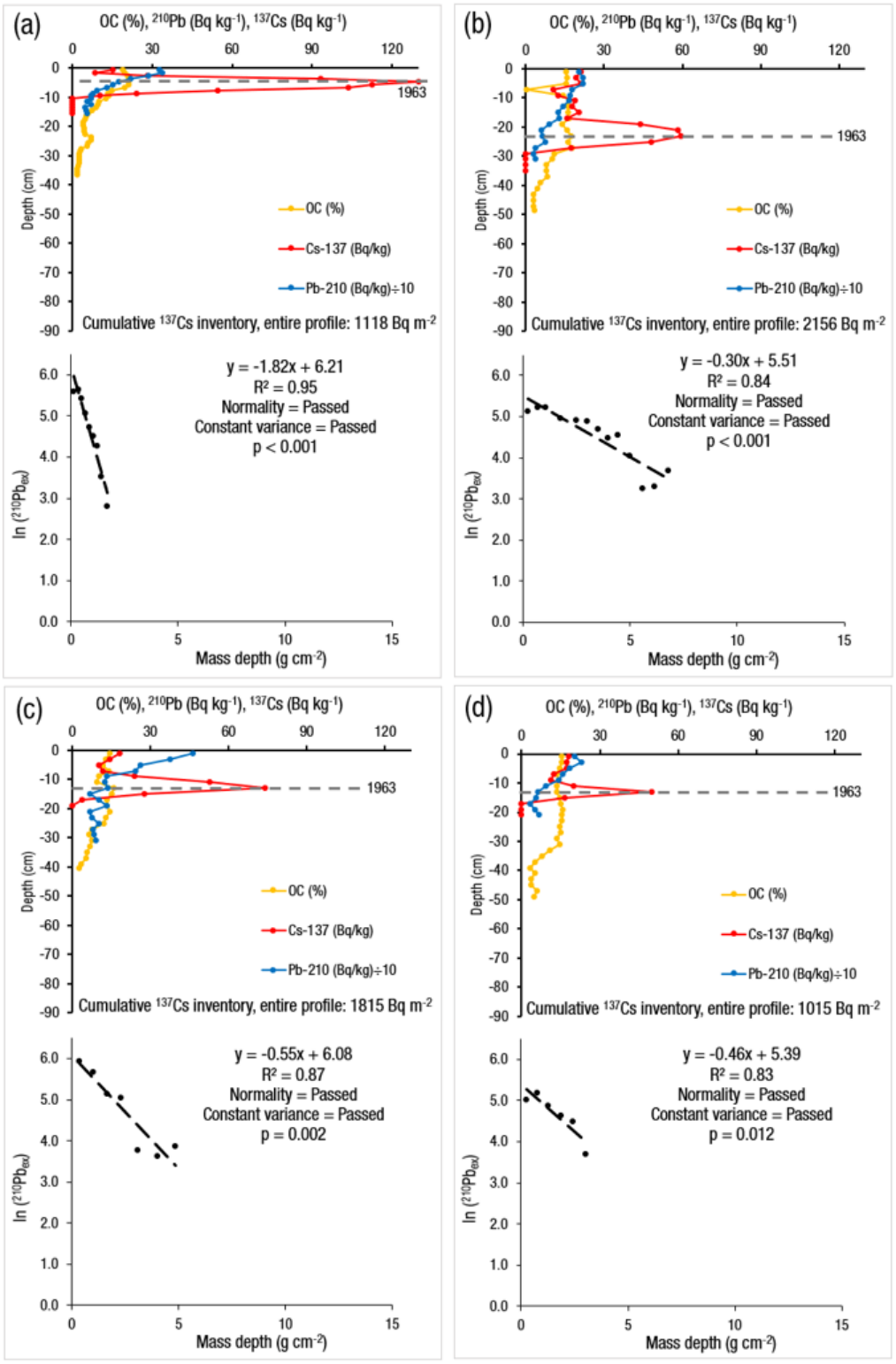

Figure S4: Depth distributions of high-quality ^{137}Cs (Bq kg^{-1}) and high-quality ^{210}Pb (Bq kg^{-1}) profiles (along with the organic carbon [OC] concentrations [%], cumulative ^{137}Cs inventory [Bq m^{-2}], and linear plot of log-transformed $^{210}Pb_{ex}$ against mass depth [g cm^{-2}]) based on their classification. The four depth distribution plots are from sediment cores (a) S-FO-I-W9-T2-CW-R2, (b) S-FO-I-W11-T1-CW-R1, (c) S-FO-I-W11-T2-CW-R2, and (d) S-FO-I-W11-T3-CW-R3.

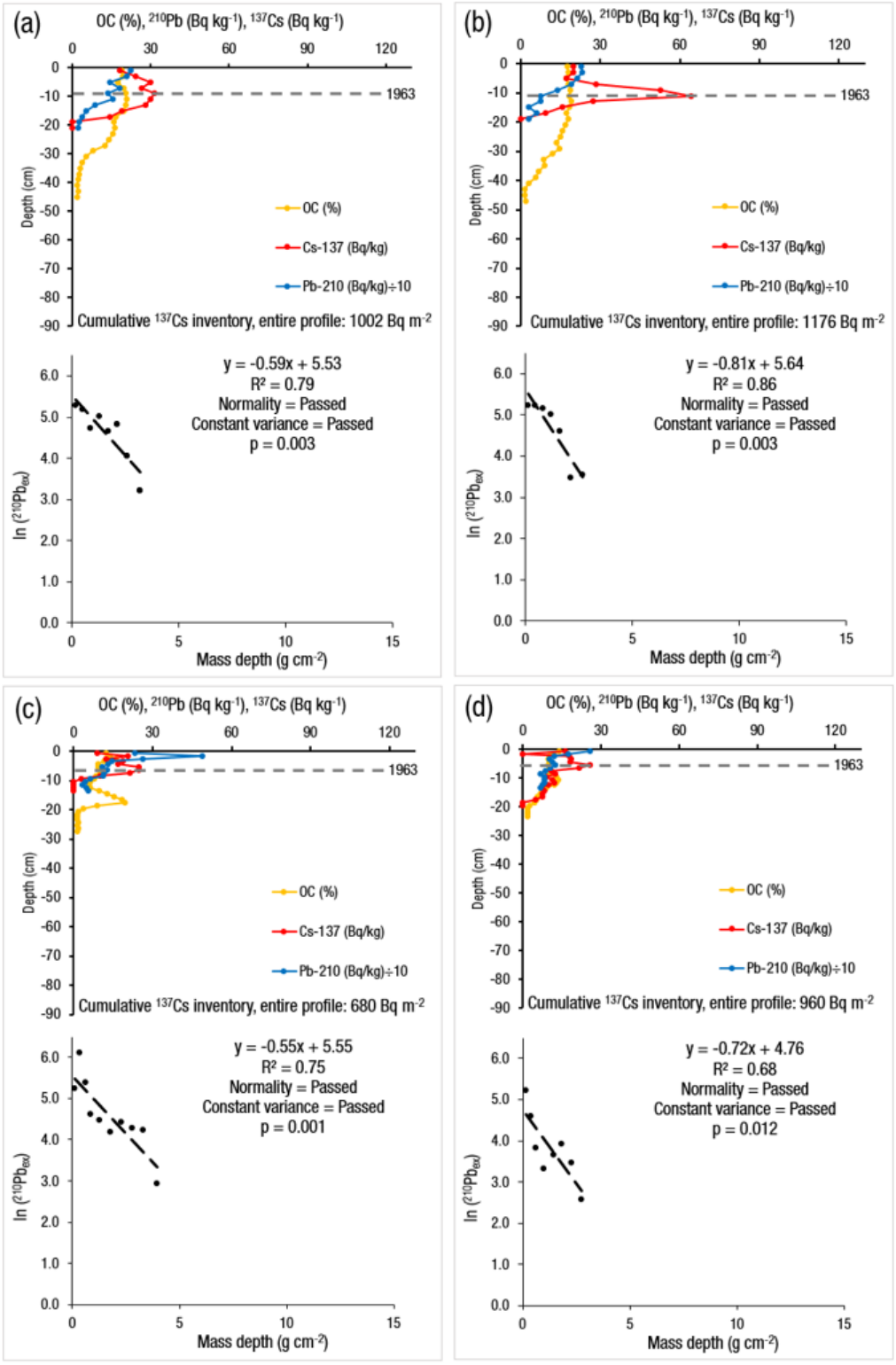

Figure S5: Depth distributions of high-quality ^{137}Cs (Bq kg^{-1}) and high-quality ^{210}Pb (Bq kg^{-1}) profiles (along with the organic carbon [OC] concentrations [%], cumulative ^{137}Cs inventory [Bq m^{-2}], and linear plot of log-transformed ^{210}Pb$_{ex}$ against mass depth [g cm^{-2}]) based on their classification. The four depth distribution plots are from sediment cores (a) S-FO-I-W12-T1-CW-R1, (b) S-FO-I-W12-T3-CW-R3, (c) S-FO-I-W16-T2-CW-R2, and (d) S-FO-I-W16-T3-CW-R3.

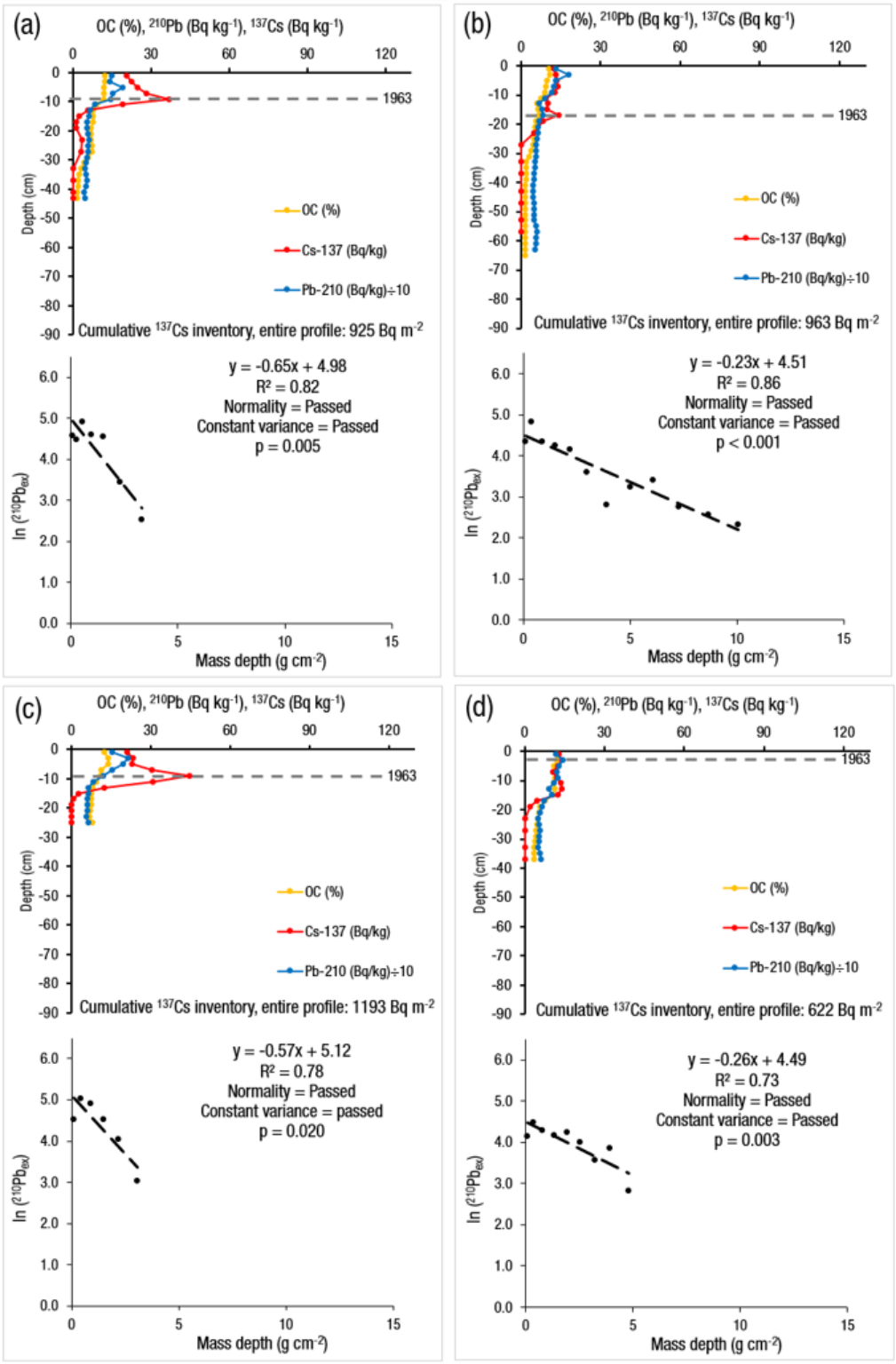

Figure S6: Depth distributions of high-quality ^{137}Cs (Bq kg^{-1}) and high-quality ^{210}Pb (Bq kg^{-1}) profiles (along with the organic carbon [OC] concentrations [%], cumulative ^{137}Cs inventory [Bq m^{-2}], and linear plot of log-transformed $^{210}Pb_{ex}$ against mass depth [g cm^{-2}]) based on their classification. The four depth distribution plots are from sediment cores (a) M-OA-I-W1-T1-CW-R1, (b) M-OA-I-W1-T2-CW-R2, (c) M-OA-I-W1-T3-CW-R3, and (d) M-OA-I-W2-T1-CW-R1.

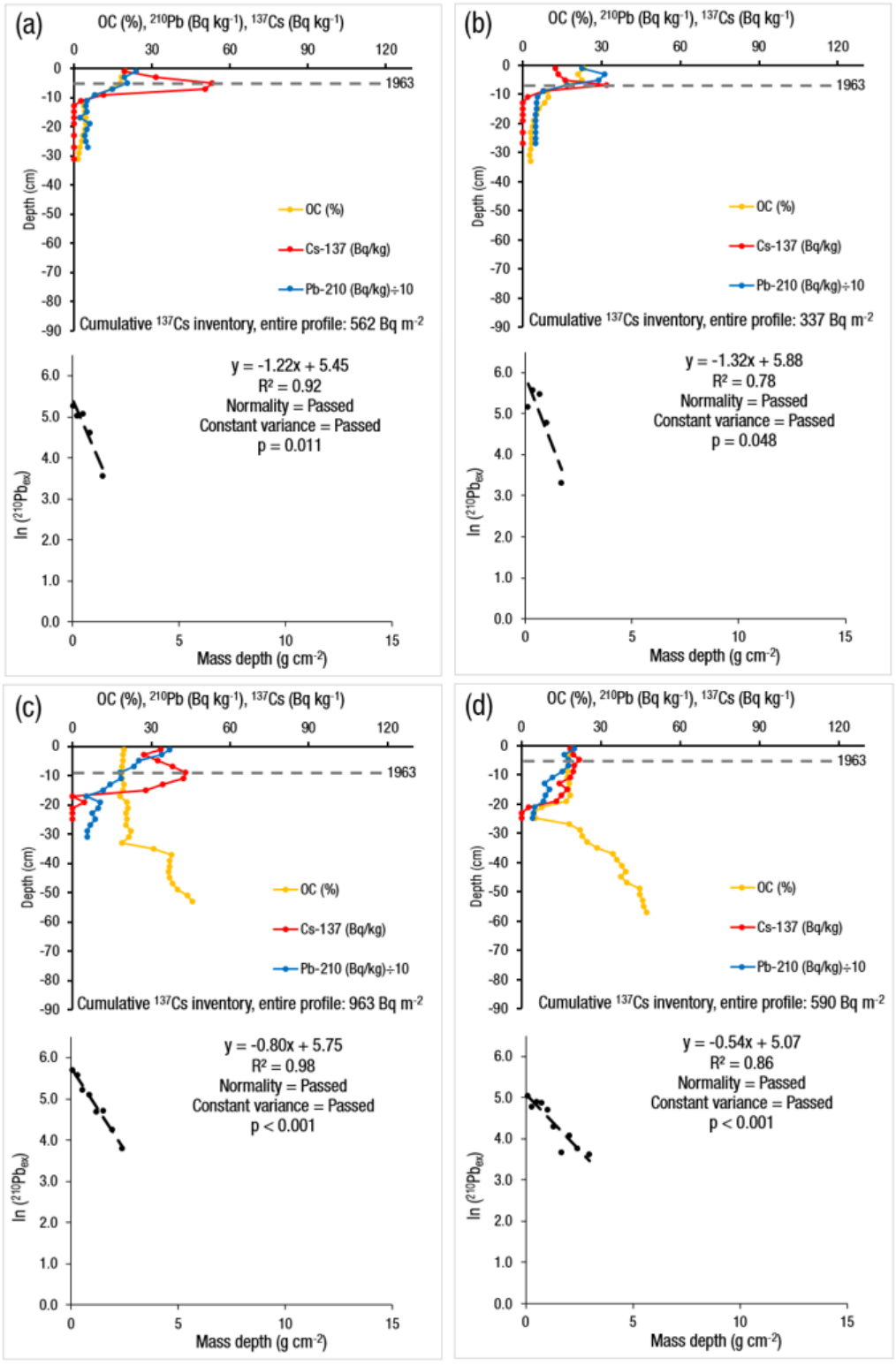

Figure S7: Depth distributions of high-quality ^{137}Cs (Bq kg^{-1}) and high-quality ^{210}Pb (Bq kg^{-1}) profiles (along with the organic carbon [OC] concentrations [%], cumulative ^{137}Cs inventory [Bq m^{-2}], and linear plot of log-transformed $^{210}Pb_{ex}$ against mass depth [g cm^{-2}]) based on their classification. The four depth distribution plots are from sediment cores (a) M-OA-I-W4-T1-CW-R1, (b) M-OA-I-W4-T2-CW-R2, (c) O-BR-I-W1-T2-CW-R2, and (d) O-BR-I-W1-T3-CW-R3.

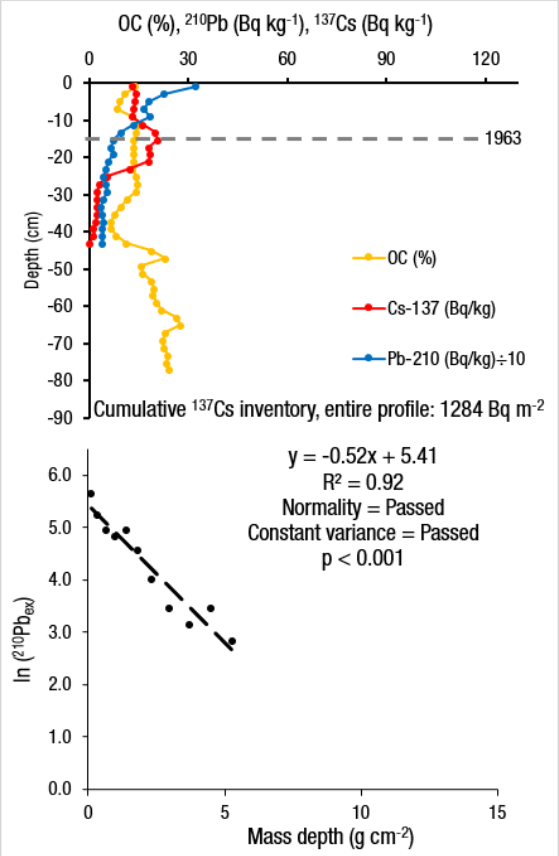

Figure S8: Depth distributions of high-quality ^{137}Cs (Bq kg^{-1}) and high-quality ^{210}Pb (Bq kg^{-1}) profiles (along with the organic carbon [OC] concentrations [%], cumulative ^{137}Cs inventory [Bq m^{-2}], and linear plot of log-transformed $^{210}Pb_{ex}$ against mass depth [g cm^{-2}]) based on their classification. The depth distribution plot is from sediment core O-AL-I-W5-T3-CW-R3.

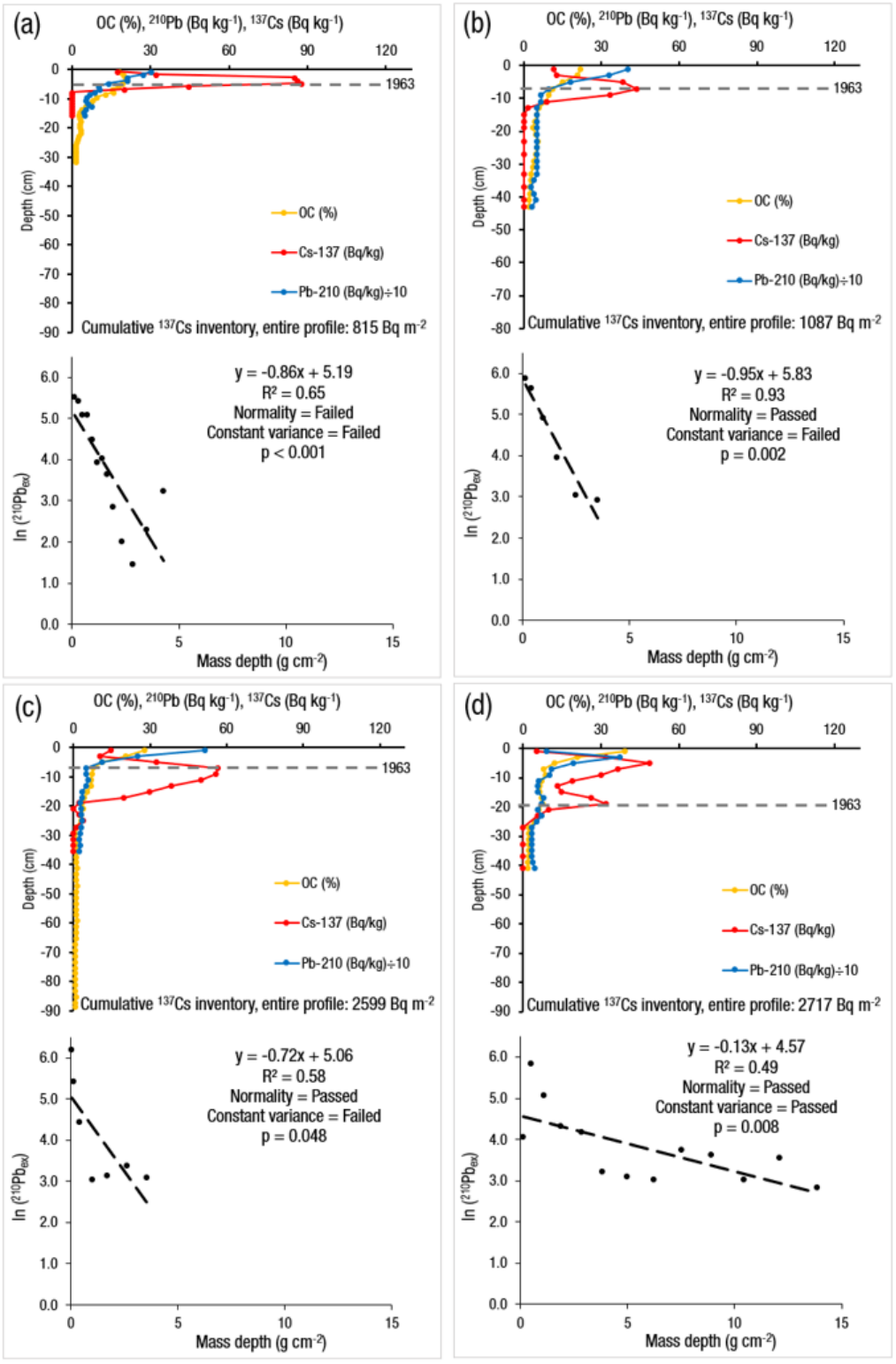

Figure S9: Depth distributions of high-quality ^{137}Cs (Bq kg^{-1}) and low-quality ^{210}Pb (Bq kg^{-1}) profiles (along with the organic carbon [OC] concentrations [%], cumulative ^{137}Cs inventory [Bq m^{-2}], and linear plot of log-transformed ^{210}Pb$_{ex}$ against mass depth [g cm^{-2}]) based on their classification. The four depth distribution plots are from sediment cores (a) S-FO-I-W9-T3-CW-R3, (b) M-OA-I-W3-T2-CW-R2, (c) M-OA-I-W5-T1-CW-R1, and (d) M-OA-I-W5-T3-CW-R3.

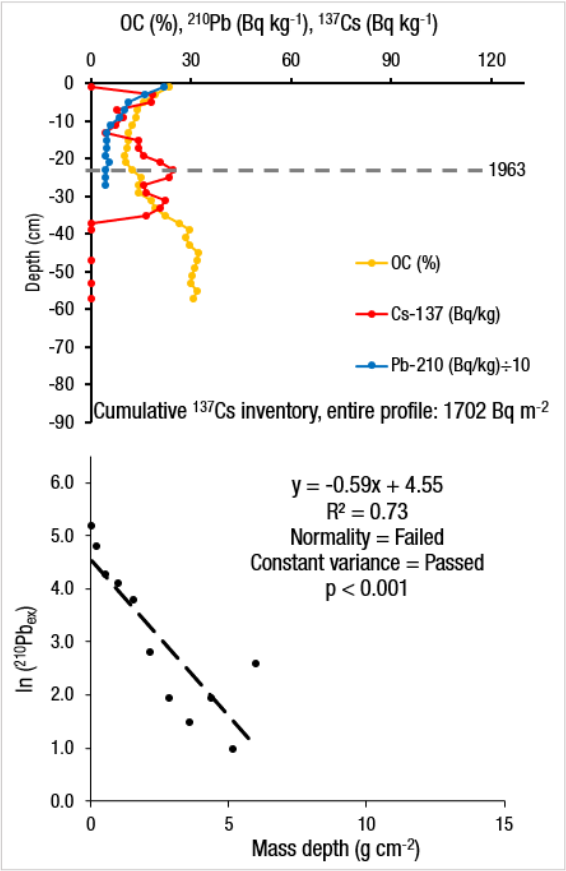

Figure S10: Depth distributions of high-quality ^{137}Cs (Bq kg^{-1}) and low-quality ^{210}Pb (Bq kg^{-1}) profiles (along with the organic carbon [OC] concentrations [%], cumulative ^{137}Cs inventory [Bq m^{-2}], and linear plot of log-transformed $^{210}Pb_{ex}$ against mass depth [g cm^{-2}]) based on their classification. The depth distribution plot is from sediment core O-AL-I-W4-T3-CW-R3.

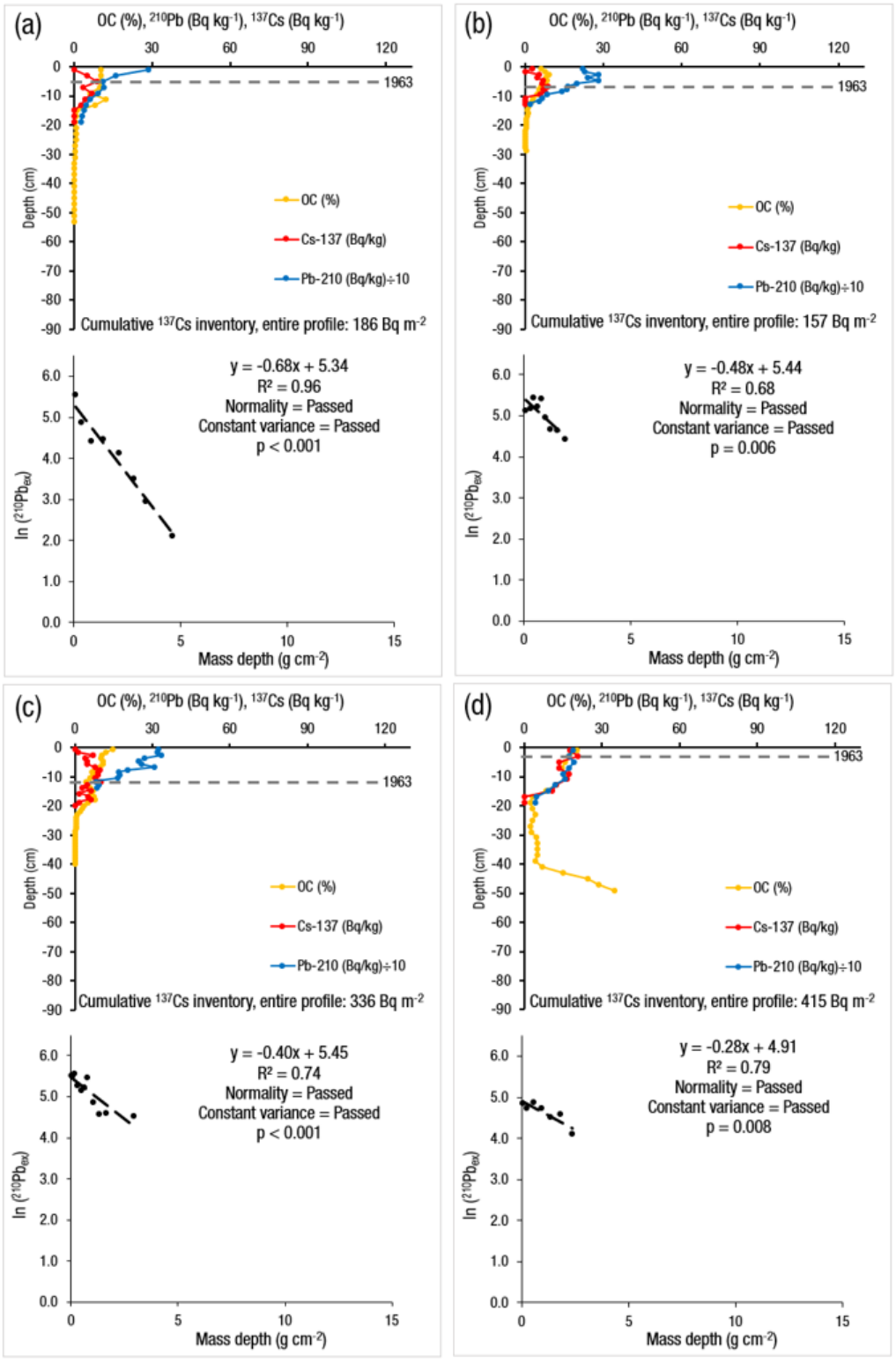

Figure S11: Depth distributions of low-quality ^{137}Cs (Bq kg^{-1}) and high-quality ^{210}Pb (Bq kg^{-1}) profiles (along with the organic carbon [OC] concentrations [%], cumulative ^{137}Cs inventory [Bq m^{-2}], and linear plot of log-transformed ^{210}Pb$_{ex}$ against mass depth [g cm^{-2}]) based on their classification. The four depth distribution plots are from sediment cores (a) O-BR-I-W2-T2-CW-R2, (b) O-BR-I-W2-T3-CW-R3, (c) O-BR-I-W2-T4-CW-R4, and (d) O-AL-I-W4-T1-CW-R1.

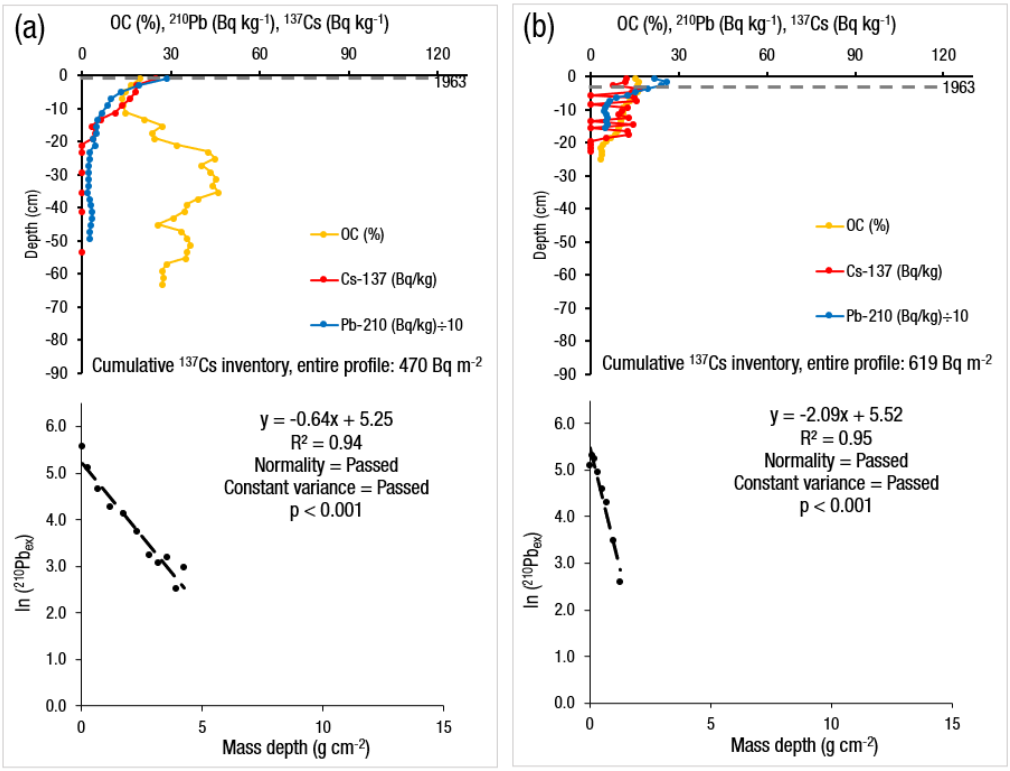

Figure S12: Depth distributions of low-quality ^{137}Cs (Bq kg^{-1}) and high-quality ^{210}Pb (Bq kg^{-1}) profiles (along with the organic carbon [OC] concentrations [%], cumulative ^{137}Cs inventory [Bq m^{-2}], and linear plot of log-transformed $^{210}Pb_{ex}$ against mass depth [g cm^{-2}]) based on their classification. The two depth distribution plots are from sediment cores (a) O-AL-I-W4-T2-CW-R2 and (b) O-AL-I-W6-T1-CW-R1.